J. Fluid Mech. (2001), *vol.* 428, *pp.* 249–272. Printed in the United Kingdom

Modelling the two-phase flow and current distribution along a vertical gas-evolving electrode

By ANDERS A. DAHLKILD

FaxénLaboratoriet, Kungliga Tekniska Högskolan, SE-100 44 Stockholm, Sweden

(Received 26 January 2000 and in revised form 28 June 2000)

The bubbly two-phase flow and electric current density distribution along a single, vertical, gas-evolving electrode are modelled and the results of a boundary layer analysis are presented. Existing empirical models for particle transport in sheared and sedimenting suspensions are adopted for the bubble mixture to close the two-phase model. Ionic species concentrations are shown to be essentially homogeneous as the mixing effect of the bubble suspension usually is much larger than dispersion by molecular diffusion even at laminar flow conditions. The non-uniformity of the bubble distribution along the electrode results in a non-uniform current density distribution, which agrees well with existing experimental findings in the literature.

1. Introduction

Gas-evolving electrodes frequently occur in industrial applications of electrochemical processes, as well as increasingly being the subject of basic research in chemical engineering. An industrial example is the chlorate process where sodium chlorate is produced under the development of hydrogen and oxygen gas. Mostly, an electrode and its counter electrode are positioned vertically, i.e. with the largest reactive surface facing the horizontal direction. The evolved gas is thus free to move-upwards so as not to accumulate on any of the electrodes. Nevertheless, the presence of gas, often in the form of small bubbles, and its motion have great impact on the performance of the electrode. A description of the phenomena involved, both from an electrochemical and a fluid dynamical point of view, is given below.

A general description of gas-evolving electrodes, and the state of the art of modelling such systems, is given by Vogt (1983). Of all the various regimes of gas evolution we are here interested in cases of nucleate gas evolution. This means that if the supersaturation of dissolved gas in the liquid adjacent to the electrode surface is sufficiently high, gas bubbles will form at predetermined nucleation sites on the surface. The bubbles grow as a result of the supply of dissolved gas from the electrolyte. In the nucleation regime, the gas bubbles leave their nucleation sites when they reach a size at which buoyancy and shear forces of the liquid are large enough to exceed the interfacial tension force by which the bubbles adhere.

From a hydrodynamic point of view the problem essentially is that of describing the two-phase flow of a bubble suspension. Experimental data, describing elements of the two-phase flow in a small electrolytic cell developing hydrogen bubbles, are given by e.g. Boissonneau & Byrne (2000). Such systems often develop turbulent flow but there are also laminar regimes of practical interest. Of particular interest here are

the mechanisms for phase distribution in laminar flow. In the case of small hydrogen bubbles the bubble slip Reynolds number is, at most, of order unity, and the channel Reynolds number for flow in the narrow gap of an electrolyzer may well be below that of transition to turbulence for single-phase flow. Dispersed phases under laminar flow conditions develop a 'pseudo-turbulence' originating in the chaotic motion of the hydrodynamically interacting multi-body system. This occurs in shear flows as well as in essentially stagnant but sedimenting systems. Together with flow-induced migration forces on the dispersed phase, the pseudo-turbulence dispersal of matter determines the phase distribution. Empirical models of these effects are discussed in more detail in the formulation of the present problem, see § 2.1 below.

The presence of bubbles also decreases the effective electric conductivity of the electrolyte by reducing the cross-sectional area of pure electrolyte available for current transport. The resulting distribution of current density along the electrodes, see figure 1, is of great importance in industrial applications. Experimental findings are summarized by Vogt (1983), including e.g. those of Hine & Murakami (1980), who measure the current density for forced and natural circulation in an electrolytic cell. Due to the enrichment of bubbles along the channel, the current density decreases rapidly from the bottom inlet to the outlet. Models in the electrochemical literature, such as in the frequently referenced work by Tobias (1959), usually assume plug flow and a uniform void fraction in each horizontal section of the narrow gap between two electrodes, that varies in the vertical direction. Vogt (1981) concludes that a non-uniform bubble distribution at each horizontal section probably is necessary to correctly model the resistivity of the electrolytic cell.

The interelectrode potential drop, and hence the current density, are also strongly influenced by the electrode overpotential, which stems from energy barriers in the charge transfer mechanisms of the electrode kinetics (see e.g. Byrne *et al.* 1999). The cumulative effect of varying electrode overpotential and the increased resistance of bubbly electrolytes on the current distribution seem to be sparsely investigated in the literature. Simplified, one-dimensional theories are given by Funk & Thorpe (1969), Rousar (1969) and Rousar *et al.* (1977).

Mass transfer of other non-gaseous species, the efficiency of which is important to the electrochemical performance of the electrode, increases with increasing current density, although the bubbles cover an increasing part of the electrode surface. State of the art models in the electrochemical literature of mass transfer due to the global convective flow caused by the buoyant bubble–liquid mixture near the electrode are usually based on the mass transfer equation for natural turbulent convection at plane walls. The pseudo-turbulence, induced by the dispersed phase, is also present in the continuous phase and may drastically influence mass transfer properties of dissolved molecular species even for overall laminar flow cases.

In the present paper we extend previous work on gas-evolving electrodes, which generally assume one-dimensional flow, by using the state of the art, dispersed two-phase flow modelling for a mono-sized suspension of spherical bubbles. The geometry is simplified in that we only consider a single vertical electrode along which a buoyant boundary layer of bubbles appears. The flow is assumed to be laminar. Faraday's law couples the production of gas at the electrode to the electric current density which is dependent on the overpotential at the electrode–electrolyte interface. Determination of the overpotential requires consideration of potential drop and charge transport in the bubbly electrolyte. Mass transport of dissolved species due to pseudo-turbulence is shown to effectively keep the species concentrations close to their bulk values. Computed current density distributions, for the single electrode considered here,

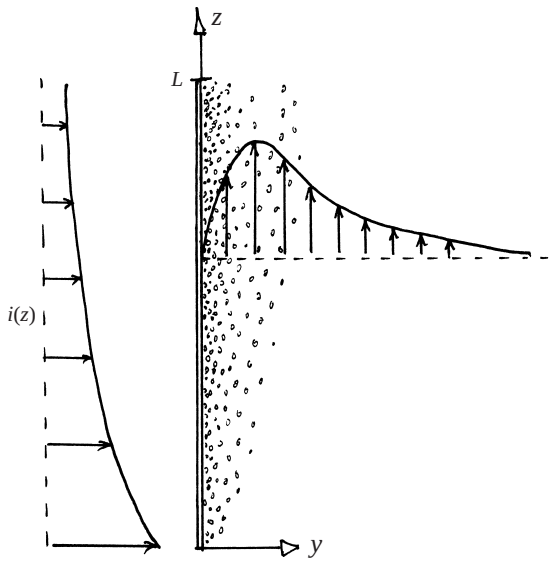

FIGURE 1. Sketch of geometry and basic phenomena.

compare well with the experiments of Hine & Murakami (1980) performed in a complete cell with natural circulation.

2. Formulation

We consider an infinite electrolyte in a two-dimensional geometry with a single vertical electrode of length L, through which flows a current density $i(z)$ as sketched in figure 1. The counter electrode is thus assumed to be sufficiently far away so as to be of negligible influence on the flow. The prototype system chosen is a binary alkaline solution of e.g. water and caustic soda with nickel as the electrode material, for which the hydrogen evolution mechanism is relatively well established, see Lukowzew, Lewina & Frumkin (1939). Our task is to determine the current density distribution along the electrode, effectuated by the non-uniform conductivity of the buoyant mixture of electrolyte and evolved gas and accounting for the variable charge transfer overpotential. The resistivity of the electrode is assumed infinitely small such that electric potential variation in the electrode is negligible compared to the overpotential and the potential drop in the bubbly electrolyte. To complete the formulation for the full fluid dynamic two-phase flow problem, § 2.1, here coupled to the ionic mass transfer in the electrolyte, § 2.2, details of electrode kinetics for hydrogen production, which is only briefly explained here in § 2.2 are given by e.g. Bockris & Reddy (1977, pp. 1231–1251), Vetter (1967, pp. 105–157, 517–536), or Lukowzew *et al.* (1939) and, specifically for this formulation, by Dahlkild (2000).

2.1. *Two-phase flow*

The evolved hydrogen is assumed to form a dispersed gaseous phase of bubbles within the continuous liquid electrolyte. To model the flow of this mixture along the electrode, we use the 'mixture' formulation, or 'diffusion' model of two-phase laminar flow (see e.g. Ishii 1975). This assumes that the liquid–bubble mixture effectively behaves as a Newtonian fluid, with a density and an effective viscosity relative to the liquid phase depending only on the volume fraction of bubbles, α. The motion of the

dispersed phase relative to the mixture, or the 'diffusion' velocity, is given separately by a constitutive law based on empirical relations described later in this section. This kind of simplified theory of two-phase flow is successfully applied to problems of sedimenting suspensions of particles, as e.g. illustrated by Acrivos & Herbolzheimer (1979). The theory is most suitable for cases when the diffusion velocity is small in comparison to the mixture velocity and inertial effects on the relative motion of the phases are negligible. This is certainly not the case for all bubbly flows, but may be applicable here essentially since the bubbles are small. The diameter of departing electrolytically produced hydrogen bubbles is generally in the range of 50–100 μm (see e.g. Vogt 1983). In water, and for a bubble diameter of 50 μm, the bubble Reynolds number is 0.1 based on the terminal velocity for a single bubble in a quiscent fluid.

The density of the mixture is

$$\rho = \alpha\rho_D + (1-\alpha)\rho_C \tag{2.1}$$

where subscripts C and D denote the densities of the continuous and dispersed phases, respectively. Let $\boldsymbol{j} = (j_y, j_z)$ and $\boldsymbol{q} = (v, w)$ denote volume-averaged and mass-averaged flux densities of the mixture, given by

$$\boldsymbol{j} = \boldsymbol{j}_D + \boldsymbol{j}_C, \quad \rho\boldsymbol{q} = \rho_D\boldsymbol{j}_D + \rho_C\boldsymbol{j}_C, \quad \boldsymbol{j}_D = \alpha\boldsymbol{v}_D, \quad \boldsymbol{j}_C = (1-\alpha)\boldsymbol{v}_C, \tag{2.2a–d}$$

where $\boldsymbol{v}_D$ and $\boldsymbol{v}_C$ are the separate velocities of the two phases. Furthermore, let $\boldsymbol{j}_R$ denote the relative volume flux density of the dispersed phase, defined by

$$\boldsymbol{j}_R = \boldsymbol{j}_D - \alpha\boldsymbol{j}. \tag{2.3}$$

It then follows that $\boldsymbol{j}$ and $\boldsymbol{q}$ are related by

$$\boldsymbol{j} = \boldsymbol{q} - \frac{\epsilon}{1+\epsilon\alpha}\boldsymbol{j}_R, \quad \epsilon = (\rho_D - \rho_C)/\rho_C. \tag{2.4a,b}$$

In our case $\rho_D \ll \rho_C$, so that we may set $\epsilon = -1$. In addition, variations in ionic species concentrations are assumed to be small so that ρ_C effectively can be considered as constant throughout the electrolyte. For the relative viscosity we use

$$\frac{\mu}{\mu_C} = \mu_e(\alpha) = \frac{1}{1-\alpha} \tag{2.5}$$

which follows from an empirical relation proposed by Ishii & Zuber (1979) in the limit of vanishing gas viscosity and a maximum packing limit of the bubbles at a volume fraction of unity. The latter assumption could certainly be questioned, especially since in other aspects we will model the bubbles like solid particles, for which the packing limit is lower. However, the behaviour of a bubble foam is probably an open question even if the bubbles behave much like particles at lower concentrations. As we put less effort into the very detailed modelling here and concentrate on physical principles and major effects, (2.5) will serve the purpose of this particular study. It is worth noting that values of $\alpha \simeq 1$ do not appear in this investigation.

The governing equations of the two-phase flow, i.e. conservation of mixture and disperse-phase volume and conservation of mixture momentum, are respectively at $\epsilon = -1$ given by

$$\nabla\cdot\boldsymbol{j} = 0, \tag{2.6}$$

$$\nabla\cdot\boldsymbol{j}_D = \nabla\cdot(\alpha\boldsymbol{j}) + \nabla\cdot\boldsymbol{j}_R = 0, \tag{2.7}$$

$$\rho_C(1-\alpha)\boldsymbol{q}\cdot\nabla\boldsymbol{q} = -\nabla P + \rho_C g\alpha\hat{\boldsymbol{z}} + (\nabla\cdot[\mu(\alpha)(\nabla\boldsymbol{q} + \nabla\boldsymbol{q}^T)] - \nabla[\tfrac{2}{3}\mu(\alpha)\nabla\cdot\boldsymbol{q}]), \tag{2.8}$$

where $P = p + \rho_C g z$ is the reduced pressure.

Boundary conditions on the electrode include a no-slip condition for the tangential velocity component of the mixture, and a zero normal velocity component of the continuous phase. The former condition is an assumption which in general does not imply no-slip conditions for any of the phases separately when using the mixture model. In our case though, as we neglect the density of the disperse phase, the no-slip condition will hold for the continuous phase. Consistent with our assumption that $\epsilon = -1$, we neglect the net mass flux of the continuous phase at the boundary due to the gas-producing chemical reactions. The normal component of the volume flux density in the dispersed phase is prescribed by the local volumetric production rate of gas per unit area at the electrode, $j_{H_2}(z)$, which is determined by the local current density through Faraday's law. If all the hydrogen evolved by the electrochemical reaction is assumed to transform into gaseous phase in a layer of negligible thickness adjacent to the electrode, the local volumetric production rate of gas per unit area is

$$j_{H_2}(z) = \frac{1}{2}\frac{\mathscr{R}T}{p_{H_2}}\frac{i(z)}{F}, \tag{2.9}$$

where $i(z)$ is the current density at the electrode wall, p_{H_2} the gas pressure, T the temperature, $\mathscr{R}$ the universal gas constant and F the Faraday constant. The factor $1/2$ in (2.9) indicates the fact that two electrons must be transferred for the production of each hydrogen molecule. (Average values of the gas production rate and the current density over the electrode surface are denoted by $j_{H_2 m}$ and i_m respectively.) At large distance from the electrode, the bubble volume fraction and the vertical flow velocity both approach zero.

In order to formulate the law for the relative motion, we need to specify some properties of the disperse phase and characterize its behaviour. The detachment of bubbles from the wall are assumed to occur at a constant bubble size and at a continuous rate, as determined by the local current density. Changes in bubble size, due to varying hydrostatic pressure, may be neglected if $\rho_C g L/p_{atm} \ll 1$, where L is the electrode length and p_{atm} is the atmospheric pressure. Coalescense of bubbles that are brought in contact through the motion of surrounding liquid is not accounted for either. This seems to be an appropriate simplification for an alkaline solution containing small hydrogen bubbles (see Janssen 1978). A physical explanation as to why coalescence is hindered may be the existence of electrical repulsive forces acting between bubbles in an electrolyte, as discussed by Marrucci & Nicodemo (1967). Also, impurities may collect on the surface of small bubbles causing it to become rigid. Thus, effects of polydispersivity are not studied here. Finally, surface tension, $\mathscr{T}$, is assumed sufficiently large, compared to deforming viscous and pressure forces, to prevent bubbles from attaining anything but a spherical shape, i.e. $\mu_C \dot{\gamma} a/\mathscr{T} \ll 1$, where $\dot{\gamma}$ is the shear rate and a the bubble radius. Thus, the bubbles behave in most aspects similarly to a suspension of light solid spherical particles. Therefore, as a first approximation, we adopt transport mechanisms known to exist for particles at low particle Reynolds numbers along with laminar flow of the mixture as a whole. In the range of bubble sizes considered here, small or moderate values of the bubble Reynolds number, as suitably defined on variables of the local flow field relative to the bubble, are to be expected. The constitutive law of the relative motion applied here is thus an extension of a model applied by Nir & Acrivos (1990) for particles sedimenting on an inclined surface, and given by

$$\boldsymbol{j}_R = \hat{\boldsymbol{z}} U_s \alpha f(\alpha) - a^2 \dot{\gamma} \beta(\alpha) \nabla\alpha - a U_s f(\alpha) \boldsymbol{D} \nabla\alpha; \quad \boldsymbol{D} = \begin{pmatrix} D_\perp & 0 \\ 0 & D_\parallel \end{pmatrix}, \tag{2.10}$$

where $U_s = g a^2/3\nu_C$ and $\dot{\gamma}$ is the magnitude of the shear rate.

The first term on the right-hand side of (2.10) is the dispersed-phase flux due to the hindered terminal velocity of bubbles rising in a quiscent mixture. A common approach (see e.g. Ishii & Zuber 1979) assumes the bubbles to rise with the velocity of a single bubble in a fluid as modified by the effective viscosity and density of the mixture, whereby $f(\alpha) = (1-\alpha)/\mu_e(\alpha)$. In fact, the magnitude of this vertical transport will turn out to be small compared to the convective vertical transport and will be neglected in the final analysis.

The transport mechanism, represented by the second term of (2.10), is known as shear- induced hydrodynamic diffusion, and is provided by mutual collisions of the bubbles (or close interactions) as they are convected in the shear flow, set up by the buoyant bubble mixture close to the electrode. As shown by Leighton & Acrivos (1987*a*, *b*) for small particle Reynolds numbers the diffusivity scales with the square of the particle size times the magnitude of the shear rate, $\dot{\gamma}$. The function $\beta(\alpha) = \frac{1}{3}\alpha^2(1 + 0.5e^{8.8\alpha})$ is given by Chapman & Leighton (1991) as an empirical approximation for the non-dimensional effective diffusion coefficient. Similar models have been sucessfully applied to resuspension phenomena of particles settling due to gravity (see e.g. Schaflinger 1996). Although analogous mechanisms for bubbles have yet to be demonstrated it is our hypothesis here that similar phenomena appear in a sheared bubble–liquid mixture.

The last term on the right-hand side of (2.10) is also a diffusive flux, but not accounted for by Nir & Acrivos (1990), known as hydrodynamic self-diffusion of a settling suspension in the context of particles. Its origin is the irregular paths of hydrodynamically interacting, neighbouring bubbles as they rise in the suspension. As shown and quantified by Ham & Homsy (1988) and Nicolai *et al.* (1995), by following marked particles of settling suspensions of identical spheres, the diffusivity scales with the particle size times the average settling speed. $D_{\parallel} \sim 8$ and $D_{\perp} \sim 1$ are approximately constant and independent of α, as reported by Nicolai *et al.* (1995). Although this coefficient of self-diffusion is not identical to the collective local gradient diffusivity, for which no detailed results are reported, they appear to be of the same order of magnitude (see Davis & Hassen 1988). For the most part the hydrodynamic self-diffusion is, in our case, smaller than the shear-induced diffusion, but becomes of critical importance in the present model around locations in the flow field where the shear rate is zero.

Most likely, there are also several other dispersion mechanisms for bubbles in laminar flow not accounted for here. Migration phenomena for single particles, like the Segré–Silberberg effect of inertia-induced lateral migration of a neutrally buoyant sphere in shear flow, as treated also by e.g. Ho & Leal (1974), and the side forces on a sedimenting particle in a shear flow, as described by Saffman (1965) and Drew & Lahey (1987), are all likely to have counterparts for small bubbles. Migration phenomena of this type, for bubbles in laminar flow, have been experimentally investigated by e.g. Kashinsky, Timkin & Cartellier (1993) and Nakoryakov *et al.* (1996) and have also been treated theoretically by Achard & Cartellier (1985), Drew (1990), Antal, Lahey & Flaherty (1991) and Wedin (1999). However, these issues will also not be considered here.

2.2. *Ionic species transport*

The liquid phase is assumed to consist of a dilute solution of fully ionized caustic soda in water. This can be characterized as a binary electrolyte with no homogeneous reactions taking place in the electrolyte bulk. In alkaline solutions, the overall

heterogeneous reaction for hydrogen evolution is

$$2H_2O + 2e^- \rightarrow H_2 + 2OH^-. \tag{2.11}$$

The evolution of hydrogen is thus accompanied by the production of hydroxide ions at the electrode. Due to the electroneutrality condition the molar densities of the natrium and hydroxide ions, $[Na^+]$ and $[OH^-]$, will be equal and are denoted by c in what follows. The current density is determined by the net molar flux densities of the positive and negative ions in the electrolyte

$$\boldsymbol{i} = F(\boldsymbol{N}_+ - \boldsymbol{N}_-) = -g(\alpha)(\sigma_c \nabla\phi + F(D_+ - D_-)\nabla c), \tag{2.12}$$

where ϕ is the electric field potential and where

$$g(\alpha) = (1-\alpha)^{3/2} \tag{2.13}$$

accounts for the decreased effective electrical conductivity of the bubbly electrolyte and is frequently referred to in the electrochemical literature as the Bruggeman relation, Bruggeman (1935). D_+ and D_- are the diffusivities of the ions in the pure electrolyte with the corresponding conductivity

$$\sigma_c = \frac{F^2}{\mathscr{R}T}(D_+ + D_-)c. \tag{2.14}$$

For a binary solution it is also helpful to consider another linear combination of the species flux densities:

$$\boldsymbol{N} = \frac{D_-\boldsymbol{N}_+ + D_+\boldsymbol{N}_-}{D_+ + D_-} = c\boldsymbol{j}_C - g(\alpha)\mathscr{D}\nabla c - a^2\dot{\gamma}\beta_s(\alpha)\nabla c. \tag{2.15}$$

The first term is merely the convection of ions in the liquid phase. The second term is the apparent molecular diffusion of the binary electrolyte where $\mathscr{D} = 2D_+D_-/(D_+ + D_-)$. The last term on the right-hand side of (2.15) represents the diffusion corresponding to liquid tracer diffusivities in a sheared suspension of particles. As desribed by Wang, Mauri & Acrivos (1996), these follow the same scaling as the shear-induced particle diffusivities of a suspension. They found, from theoretical considerations of dilute suspensions, the non-dimensional liquid tracer diffusion coefficient, β_s, within the plane of shear to be

$$\beta_s(\alpha) = 0.12\alpha^2, \tag{2.16}$$

which we shall use here as the basis for a conceptual model of the ionic mass transport induced by the random motion of the bubbles.

In principle, D_+ and D_- are functions of the solvent concentrations but are here, for the dilute electrolyte considered, taken as empirically determined constants. Conservation of the ionic species then requires

$$\nabla\cdot\boldsymbol{N} = 0, \quad \nabla\cdot\boldsymbol{i} = 0. \tag{2.17a,b}$$

Separate boundary conditions at the electrode for the two normal components of the ion flux densities are formulated. Since the positive ions do not take part in the chemical reaction at the electrode surface they are neither consumed or produced there, so that $\boldsymbol{N}_+\cdot\hat{\boldsymbol{y}} = 0$. The negative hydroxide ions are produced at the surface, carrying all the charge transport from the surface, i.e. $-F\boldsymbol{N}_-\cdot\hat{\boldsymbol{y}} = -i(z)$, where $i(z)$ is the, as yet undefined, distribution function for the current density at the electrode

surface. It then follows, together with the definition of the combined flux density, that

$$\boldsymbol{N}\cdot\hat{\boldsymbol{y}} = \frac{i(z)}{F}\frac{D_+}{D_+ + D_-}, \quad \boldsymbol{i}\cdot\hat{\boldsymbol{y}} = -i(z). \tag{2.18a,b}$$

The behaviour of the current density at large distances from the electrode generally requires more specific conditions of the surroundings, which is not necessary here as will be seen when we proceed with the boundary layer analysis in § 3.

To complete the formulation we need a relation between the electric potential at the electrode and the current density as determined by electrode kinetics. For a sufficiently large cathodic polarization, such that $|(F/\mathscr{R}T)\eta| \gg 1$ where the overpotential $\eta < 0$, the net current density is approximated by

$$i_y = -i^o(1-\alpha_l)\,\exp\left(-\frac{F}{2\mathscr{R}T}\eta\right), \tag{2.19}$$

Vetter (1967, p. 535). Without loss of generality the cathodic overpotential can be set equal to minus the electrolyte potential evaluated adjacent to the electrode surface, $\eta = -\Phi_l$. In (2.19) i^o is the so-called apparent exchange current density, the value of which is not essential in what follows. The factor $(1-\alpha_l)$ is introduced here, as a not unresonable approximation, to account for the reduction of the active electrode area caused by bubbles adhering to the electrode. This reduction is thus assumed to be directly proportional to the local void fraction at the electrode, α_l. An alternative would be to use some empirical relationship for this reduction which, to the present knowledge of the author, does not exist. A problem for the complete cell can be formulated either in terms of a specified cell overvoltage or a specified total current, where in the latter case the cell overvoltage appears as part of the solution. In our case, with a single electrode, only the current can be specified and the cell overvoltage will remain indeterminate. With an average current density i_m over the electrode, (2.19) may be expressed

$$i_y(z) = -i_m\frac{(1-\alpha_l(z))\exp\left(\dfrac{F}{2\mathscr{R}T}\phi_l(z)\right)}{\dfrac{1}{L}\displaystyle\int_0^L (1-\alpha_l(z))\exp\left(\frac{F}{2\mathscr{R}T}\phi_l(z)\right)\mathrm{d}z} \equiv -i(z), \tag{2.20}$$

where $\phi_l = \Phi_l - \Phi_0$ is the part of the electrolyte potential corresponding to the deviation of the current density on the electrode from its average value. Φ_0 is a constant satisfying

$$i^o\,\exp\left(\frac{F}{2\mathscr{R}T}\Phi_0\right)\frac{1}{L}\int_0^L (1-\alpha_l(z))\,\exp\left(\frac{F}{2\mathscr{R}T}\phi_l(z)\right)\mathrm{d}z = i_m. \tag{2.21}$$

As such, Φ_0 is an uninteresting quantity, as far as the mass transfer is concerned, and the problem may be formulated in terms of ϕ_l alone, where (2.20) serves as a basis for the boundary conditions of ionic species flux densities in the electrolyte as discussed previously in this section. Equation (2.20) also sets the magnitude of the gas-evolution rate through (2.9).

2.3. *Non-dimensional parameters*

Non-dimensional variables, without change of notation, are introduced using L, j_{H_2m}, ρ_C, μ_C, $\rho_C g L$ as typical values of length, velocity, density, viscosity and pressure, where L is the length of the electrode, and c_0, $c_0 j_{H_2m}$, i_m and $i_m L/\sigma_C^0$ for ion concentration,

ion molar flux density, current density and electric potential, respectively. The non-dimensional parameters are

$$\Lambda_L = \frac{gL^2}{\nu_C j_{H_2 m}}, \quad \Lambda_a = \frac{ga^2}{\nu_C j_{H_2 m}}, \quad Re_L = \frac{j_{H_2 m} L}{\nu_C}, \tag{2.22}$$

where ν_C is the kinematic viscosity of the continuous phase, and

$$Pe_L = \frac{j_{H_2 m} L}{\bar{D}}, \quad \Delta D = \frac{D_+ - D_-}{D_+ + D_-}, \quad X_0 = \frac{c_0 \mathscr{R} T}{p_{H_2}}, \tag{2.23}$$

where $\bar{D} = (D_+ + D_-)/2$. With this scaling of variables, Λ_L is the ratio of buoyancy and viscous forces and $\Lambda_a = 3U_s/j_{H_2 m}$ is the ratio of the modified Stokes velocity and the gas injection velocity. In the boundary layer analysis, see § 3 below, Λ_a turns out to be the relative measure for the shear-induced bubble flux magnitude in the wall-normal direction.

3. Analysis

Values of Λ_L and Pe_L are typically very large. For an average current density of $2000\,\mathrm{A\,m^{-2}}$, an electrode length of 0.5 m and a kinematic viscosity and molecular diffusivity of $10^{-6}\,\mathrm{m^2\,s^{-1}}$ and $10^{-9}\,\mathrm{m^2\,s^{-1}}$ respectively, we obtain values in the order of $\Lambda_L \sim 10^{10}$ and $Pe \sim 10^5$ and a Reynolds number $Re_L \sim 10^2$. This indicates that we can expect characteristics of a boundary layer in the flow along the electrode. Thus, there will be a thin bubble plume close to the electrode, decreasing the conductivity of the electrolyte, but increasing the effective mass transport of ions in relation to a pure electrolyte. A boundary layer analysis is presented next where we show that if Λ_a is sufficiently large, mass transport due to the shear-induced diffusion will be large enough to keep the ion concentration, in the greater part of the bubble plume, at values close to that in the bulk.

If one disregards the ionic mass transport, which will play a passive role here, mathematical and to some extent also physical analogies can be drawn with the well-known problem of laminar natural convection along a heated plate. The bubble plume is buoyant, like the heated fluid, but unlike the heated fluid the plume is also a source of volume at the wall since the relative density differences in the plume are much larger than usually considered for the heated fluid. $\Lambda_L \gg 1$ plays the role of a Grashof number and the Prandtl number would be $\nu_C/U_s a \gg 1$ measuring the ratio of the diffusivities of momentum and hydrodynamic self-diffusion. This ratio, however, plays a minor role for the plume since the dominating transport mechanism of the bubbles are shear-induced diffusion and convection. Thus, a ratio for our problem, with similar role to the Prandtl number for the heated plate, would be $\nu_C/a^2\dot{\gamma}$, which will turn out to be fairly large in what follows. The structure of the boundary layer for the plume is therefore expected to have some similarities with that for a heated plate at large Prandtl numbers, such as a buoyant viscous inner layer and an inertial, essentially non-buoyant outer layer.

3.1. *Boundary layer approximations*

The thickness of the hydrodynamic boundary layer, δ, may be estimated from an assumed balance between buoyancy and viscous forces in the vertical component of (2.8) through which $\delta^2 \sim w/\Lambda_L$. As, supposedly, $v \sim 1$ it follows from continuity that $w \sim 1/\delta$ so that $\delta \sim \Lambda_L^{-1/3} \ll 1$. New boundary layer variables are then introduced

according to

$$\tilde{w} = w\Lambda_L^{-1/3}, \quad \tilde{v} = v, \quad \tilde{j}_z = j_z\Lambda_L^{-1/3}, \quad \tilde{j}_y = j_y, \quad \tilde{\phi} = \phi\Lambda_L^{1/3}, \quad \tilde{y} = y\Lambda_L^{1/3}. \quad (3.1a\text{–}f)$$

Introducing these new variables into the governing equations, through formally considering the limit

$$\Lambda_L \to \infty, \quad Re_L\Lambda_L^{-1/3} \sim 1, \quad Pe_L\Lambda_L^{-1/3} \sim 1, \quad \Lambda_a \sim 1, \tag{3.2}$$

and neglecting all terms of order $\Lambda_L^{-1/3}$ or smaller, shows that the vertical component of the relative velocity may be neglected in comparison with the vertical advection of particles. With the same order of accuracy we may set $\tilde{w} = \tilde{j}_z$ whereas for the wall-normal component we have $\tilde{v} = \tilde{j}_y - \tilde{j}_{Ry}/(1-\alpha)$ with $\tilde{j}_{Ry}/(1-\alpha) \sim 1$. The boundary layer equations, retaining only terms of relative orders larger than $\Lambda_L^{-1/3}$, are

$$\frac{\partial \tilde{j}_z}{\partial z} + \frac{\partial \tilde{j}_y}{\partial \tilde{y}} = 0, \tag{3.3}$$

$$\frac{\partial}{\partial z}(\alpha\tilde{j}_z) + \frac{\partial}{\partial \tilde{y}}(\alpha\tilde{j}_y) = \Lambda_a \frac{\partial}{\partial \tilde{y}}\left(\beta(\alpha)\left|\frac{\partial \tilde{j}_z}{\partial \tilde{y}}\right|\frac{\partial \alpha}{\partial \tilde{y}} + \frac{1}{3}\frac{\Lambda_a^{1/2}}{\Lambda_L^{1/6}}D_\perp\frac{\partial \alpha}{\partial \tilde{y}}\right), \tag{3.4}$$

$$Re_\delta\left((1-\alpha)\tilde{j}_z\frac{\partial \tilde{j}_z}{\partial z} + [(1-\alpha)\tilde{j}_y - \tilde{j}_{Ry}]\frac{\partial \tilde{j}_z}{\partial \tilde{y}}\right) = \alpha + \frac{\partial}{\partial \tilde{y}}\left(\mu_e(\alpha)\frac{\partial \tilde{j}_z}{\partial \tilde{y}}\right), \tag{3.5}$$

$$(1-\alpha)\tilde{j}_z\frac{\partial c}{\partial z} + [(1-\alpha)\tilde{j}_y - \tilde{j}_{Ry}]\frac{\partial c}{\partial \tilde{y}} = \frac{1-\Delta D^2}{Pe_\delta}\frac{\partial}{\partial \tilde{y}}\left(g(\alpha)\frac{\partial c}{\partial \tilde{y}}\right) + \Lambda_a\frac{\partial}{\partial \tilde{y}}\left(\left|\frac{\partial \tilde{j}_z}{\partial \tilde{y}}\right|\beta_s(\alpha)\frac{\partial c}{\partial \tilde{y}}\right), \tag{3.6}$$

where

$$\tilde{j}_{Ry} = -\Lambda_a\left(\beta(\alpha)\left|\frac{\partial \tilde{j}_z}{\partial \tilde{y}}\right|\frac{\partial \alpha}{\partial \tilde{y}} + \frac{1}{3}\frac{\Lambda_a^{1/2}}{\Lambda_L^{1/6}}D_\perp\frac{\partial \alpha}{\partial \tilde{y}}\right) \tag{3.7}$$

and

$$\frac{\partial \tilde{i}_y}{\partial \tilde{y}} = 0, \quad \tilde{i}_y = -cg(\alpha)\frac{\partial \tilde{\phi}}{\partial \tilde{y}} - \frac{\Delta D}{Pe_\delta}X_0 g(\alpha)\frac{\partial c}{\partial \tilde{y}}, \tag{3.8}$$

and where we have introduced

$$Re_\delta = Re_L\Lambda_L^{-1/3}, \quad Pe_\delta = Pe_L\Lambda_L^{-1/3}. \tag{3.9}$$

(One may infer that $Re_\delta \sim a^2\dot{\gamma}/\nu_C$ and thereby has the role of an inverse Prandtl number as discussed in the previous paragraph.) The boundary conditions at the electrode are

$$\tilde{j}_z(\tilde{y}=0) = 0, \quad \tilde{j}_y(\tilde{y}=0) = \left(\frac{\tilde{j}_{Ry}}{(1-\alpha)}\right)_{\tilde{y}=0} = i(z), \tag{3.10}$$

$$-\left(\frac{1-\Delta D^2}{Pe_\delta}g(\alpha)\frac{\partial c}{\partial \tilde{y}} + \Lambda_a\left|\frac{\partial \tilde{j}_z}{\partial \tilde{y}}\right|\beta_s(\alpha)\frac{\partial c}{\partial \tilde{y}}\right)_{\tilde{y}=0} = \frac{1+\Delta D}{X_0}i(z), \tag{3.11}$$

$$\tilde{i}_y(\tilde{y}=0) = -i(z), \tag{3.12}$$

where

$$i(z) = \frac{(1-\alpha_l(z))\exp\left(\dfrac{Pe_\delta}{2X_0}\tilde{\phi}_l(z)\right)}{\displaystyle\int_0^1 (1-\alpha_l(z))\exp\left(\frac{Pe_\delta}{2X_0}\tilde{\phi}_l(z)\right)\mathrm{d}z}. \tag{3.13}$$

Far away from the electrode

$$\tilde{j}_z(\tilde{y}\to\infty)\to 0, \quad \alpha(\tilde{y}\to\infty)\to 0, \quad c(\tilde{y}\to\infty)\to 1. \tag{3.14}$$

At the lower end of the electrode there is no oncoming flow and also no bubbles so that

$$\tilde{j}_z(z=0)=0, \quad \alpha(z=0)=0, \quad c(z=0)=1. \tag{3.15}$$

It follows from (3.8) and (3.12) that the horizontal component of the current density is constant through the boundary layer and that far away from the electrode

$$\tilde{i}_y = -\frac{\partial\tilde{\phi}}{\partial\tilde{y}} = -i(z). \tag{3.16}$$

We then introduce the ansatz

$$\tilde{\phi} = i(z)\tilde{y} + \tilde{\phi}', \tag{3.17}$$

where

$$\tilde{\phi}'(\tilde{y}\to\infty)\to 0. \tag{3.18}$$

Substituting the ansatz (3.17) into (3.8) and integrating yields

$$\tilde{\phi}_l = \tilde{\phi}'_l = -\frac{\Delta D}{Pe_\delta}X_0\ln c_l - i(z)\int_0^\infty \frac{1-cg(\alpha)}{cg(\alpha)}\,\mathrm{d}\tilde{y}, \tag{3.19}$$

where again the subscript l denotes evaluation in the liquid electrolyte at $\tilde{y}=0$. The first term on the right-hand side of (3.19) is usually termed the *diffusion overpotential*. The second term could be denoted the *bubble overpotential*, as it is caused by the increase in reduced resistivity of the thickening boundary layer brought about by the presence of the bubbles. Equation (3.19) is an implicit relation for $\tilde{\phi}_l$ since $i(z)$, by (3.13), depends on $\tilde{\phi}_l$. Alternatively, by substituting (3.19) into (3.13) we obtain an implicit relation for $i(z)$.

We shall specify typical values of the non-dimensional parameters in order to estimate the variation of ionic species concentration in the boundary layer. Consider bubbles of radius $a = 50\,\mu\mathrm{m}$, an electrode of length $L = 0.5\,\mathrm{m}$, an electrolyte kinematic viscosity $\nu = 10^{-6}\,\mathrm{m^2\,s^{-1}}$, diffusivities of the ionic species $D_+ = 1.33\times10^{-9}\,\mathrm{m^2\,s^{-1}}$ and $D_- = 5.27\times10^{-9}\,\mathrm{m^2\,s^{-1}}$, corresponding to molar conductivities of 5.01 and $19.8\,\mathrm{S\,m^2\,kg^{-1}}$ mole respectively (see Atkinson 1972), a temperature of $T = 300\,\mathrm{K}$, a gas pressure of $p_{H_2} = 10^5\,\mathrm{Pa}$ and an average current density of $i_m = 2000\,\mathrm{A\,m^{-2}}$. We then obtain $\Lambda_a = 94.9, Re_\delta = 0.06, Pe_\delta = 18.5, \Lambda_L = 94.9\times10^8$ and with a bulk concentration $c_0 = 0.4\,\mathrm{kg\,mole\,m^{-3}}$, $X_0 = 10$. It then follows from (3.6), by comparing the orders of magnitude of the two terms on the right-hand side, that the dominating mass transport mechanism, relative to the continuous-phase transport, is that due to shear-induced tracer diffusion in the bubble suspension. Under the assumption that shear-induced diffusion is dominant in (3.4) also, $\tilde{j}_z \sim \Lambda_a\beta\tilde{j}_z/\tilde{\delta}^3$, where $\tilde{\delta}$ is an estimate of the boundary layer thickness in the scaled coordinate. Considering a balance between buoyancy and viscous forces in (3.5) gives $\alpha \sim \tilde{j}_z/\tilde{\delta}^2$ and from the boundary conditions (3.10), (3.11), we find $\Lambda_a\beta\tilde{j}_z\alpha/\tilde{\delta}^2 \sim 1$ and $\Lambda_a\beta_s\tilde{j}_z\Delta c/\tilde{\delta}^2 \sim 1/X_0$

where Δc is the variation of the non-dimensional ionic species concentration in the boundary layer. Then, for large Λ_a and with the estimates $\beta \sim \beta_s \sim \alpha^2$, we get $\alpha \sim \Lambda_a^{-1/4}, \tilde{j}_z \sim \Lambda_a^{1/12}, \tilde{\delta} \sim \Lambda_a^{1/6}$ and $\Delta c \sim \Lambda_a^{-1/4}/X_0$. With typical values of Λ_a and X_0 given above we obtain $\Delta c \sim 0.03 \ll 1$. Therefore, here we shall neglect any deviations of the ionic species concentration from that in the bulk, i.e. c is considered constant and equal to one. Thereby, we have eliminated one of the dependent variables and the coupling between hydrodynamics and mass transport is now only present through the boundary condition (3.10) and the effective conductivity of the suspension, $g(\alpha)$. For this reduced system of equations the Péclet number is encountered only through (3.13) in the relation $\Gamma = Pe_\delta/X_0$. This can also be written

$$\Gamma = \frac{i_m \Lambda_L^{-1/3} L/\sigma_C^0}{\mathscr{R}T/F}, \tag{3.20}$$

which estimates the ratio of the potential drop in the boundary layer and the difference in potential as the equivalent to thermal kinetic energy per unit charge.

The simplified formulation is a result of the supposed effectiveness of mass transport, induced by the bubble suspension, in comparison to molecular diffusion. One could argue though, that close to the wall, the random fluctuating motions of the bubbles are restricted, and that for a certain distance from the wall, smaller than a bubble diameter, the overall mass transport mechanism must be mainly molecular diffusion. Considering the lower efficiency of this mechanism, the value of c_l appearing in (3.19) would therefore differ from one. In fact, such a wall region is discussed by Koch (1996) for sheared suspensions of particles. Using his ideas, theoretical estimates of c_l yield significant deviations from one. On the other hand, in the case of bubbles evolving on an electrode there also exist other mass transfer mechanisms from microconvection that are of importance close to the electrode surface. In particular the effect of sliding bubbles at the wall, as reported by Janssen (1989), indicate that mass transfer close to the wall in reality is more effective than that by pure molecular diffusion. The presence of these effects, not modelled in detail here, may allow the use of the present model all the way to the wall, where its validity may be somewhat doubtful.

3.2. *Numerical procedure*

At a first glance, the system of boundary layer equations may seem to be of the standard type, in that they can be solved by a suitable marching procedure from known variable values at the lower edge of the electrode. However, one should observe that, since (3.13) involves an integration of dependent variables along the full length of the electrode, the system of equations is not strictly parabolic. The unknown at the outset is the value of the current density at $z = 0$. There are no mechanisms for bubbles to penetrate below the lower end of the electrode in the boundary layer formulation, so that there can be no bubbles present at $z = 0^-$. This means that $\alpha_l(z = 0) = 0$ and from (3.19) where $\tilde{\phi}_l(z = 0) = 0$ with $c = 1$, we obtain from (3.13)

$$i(z = 0) = \frac{1}{\displaystyle\int_0^1 (1 - \alpha_l(z)) \exp\left(\frac{\Gamma}{2}\tilde{\phi}_l(z)\right) \mathrm{d}z} \equiv i_o. \tag{3.21}$$

Thus, the current density at the lower edge of the electrode depends on the full solution along the electrode. However, if i_o was known initially, the problem would be parabolic. This observation is used here to formulate an iteration procedure (see

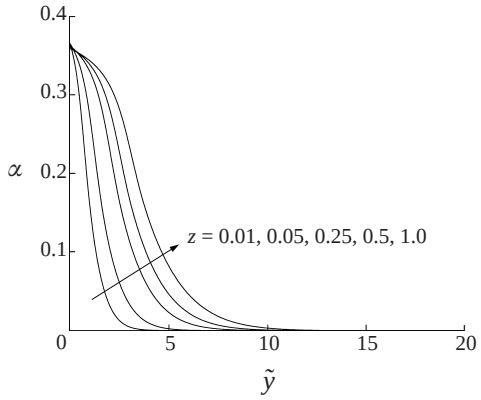

FIGURE 2. Gas volume fraction versus wall-normal coordinate at the vertical positions $z = 0.01, 0.05, 0.25, 0.5, 1.0$ for $Re_\delta = 0.06, \Lambda_a = 94.9, \Lambda_L = 94.9 \times 10^8$ and $\Gamma = 2$.

the Appendix), where an initial guess for i_o is successively updated through repeated integration of the artificially constructed parabolic system.

4. Results and discussion

Here we present results for some typical values of the non-dimensional parameters which can be thought of as representing two different bubble sizes and four different bulk concentrations. Using values of the physical variables given in the end of § 3.1, but for a bulk concentration $c_0 = 0.37\,\mathrm{kg\,mole\,m^{-3}}$, we obtain $Re_\delta = 0.06, \Lambda_a = 94.9, \Lambda_L = 94.9 \times 10^8$ and $\Gamma = 2$. With half the bubble radius, $a = 25\,\mu\mathrm{m}$, we instead get $\Lambda_a = 23.7$ but with all the other parameters unchanged. From its definition in (2.22), Λ_a is three times the ratio of the rising speed of a single bubble to the gas injection velocity. It also is an estimate of the ratio of the shear-induced flux of bubbles, in the boundary layer formulation, to that which results from advection. For the larger bubble radius, $a = 50\,\mu\mathrm{m}$, i.e. for $\Lambda_a = 94.9$, we also present results for $\Gamma = 1/2, 1$ and 4 which could be obtained by e.g. varying the bulk concentration c_0. Γ approximates the relative magnitude of the electrical potential drop through the boundary layer but for the conductivity in the abscence of bubbles.

In figure 2 the development along the electrode of the bubble volume fraction profile is shown for the case of $\Lambda_a = 94.9, \Gamma = 2$. The injected gas spreads gradually away from the electrode, keeping the volume fraction at the wall approximately constant for the vertical positions shown in figure 2. The corresponding mixture velocity profiles, as generated by the buoyant bubble layer, are shown in figure 3. As the Reynolds number is fairly low, $Re_\delta = 0.06$, an inertial layer, free from bubbles, is apparent outside the bubbly region of the velocity profiles.

The development along the electrode of the gas volume fraction at the wall, the maximum of the velocity profile and the distance from the electrode of this maximum, are shown in figure 4 for $\Lambda_a = 94.9$ and various values of Γ. As can be observed, the volume fraction appears fairly constant and essentially independent of Γ except for a region close to the lower end of the electrode. Away from the lower end, the scaling of the velocity and the boundary layer thickness also appear relevant and more or less independent of Γ.

Current density distributions for $\Lambda_a = 94.9$ and various values of Γ are shown in figure 5. Starting at the lower end, the current density first shows a rapid decrease and

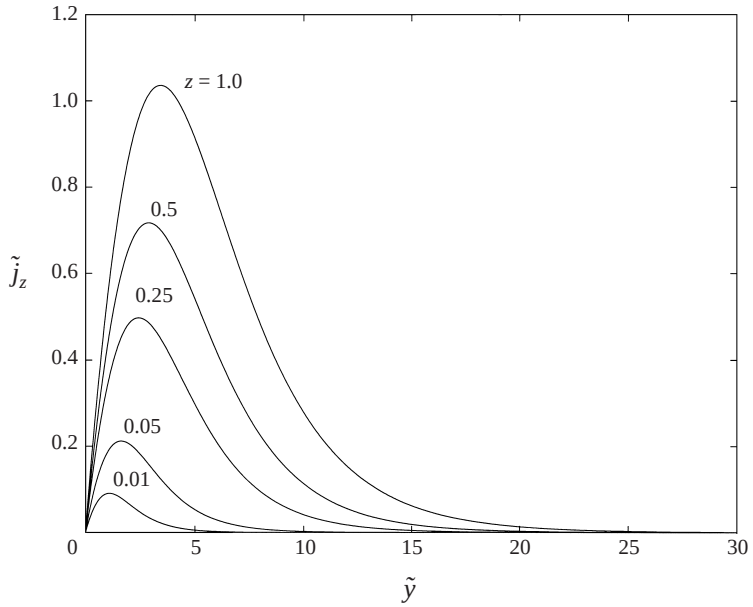

FIGURE 3. Vertical component of mixture velocity versus wall-normal coordinate at the vertical positions $z = 0.01, 0.05, 0.25, 0.5, 1.0$ for $Re_\delta = 0.06, \Lambda_a = 94.9, \Lambda_L = 94.9 \times 10^8$ and $\Gamma = 2$.

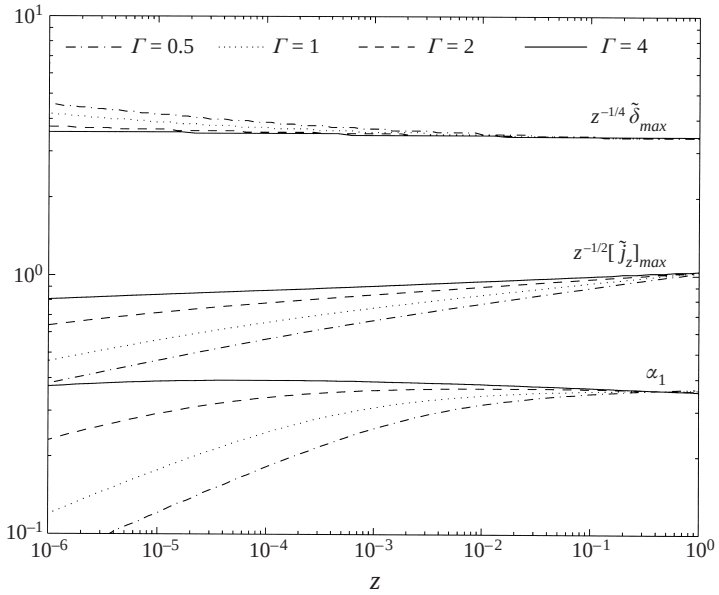

FIGURE 4. Gas volume fraction at the electrode, α_l, scaled maximum of the vertical mixture velocity profile, $z^{-1/2}[\tilde{j}_z]_{max}$, and scaled distance from the wall of the maximum velocity, $\tilde{z}^{-1/4}\tilde{\delta}_{max}$, versus the vertical coordinate for the same parameters as in figures 2 and 3 and with $\Gamma = 0.5, 1, 2, 4$.

then levels out to a smaller slope on the major part of the electrode. This decaying behaviour reflects the increased resistivity of the thickening bubble boundary layer along the electrode. For increasing values of Γ, the current density at $z = 0$, i_o, increases as shown in table 1. Thus, increasing Γ gives a more uneven current

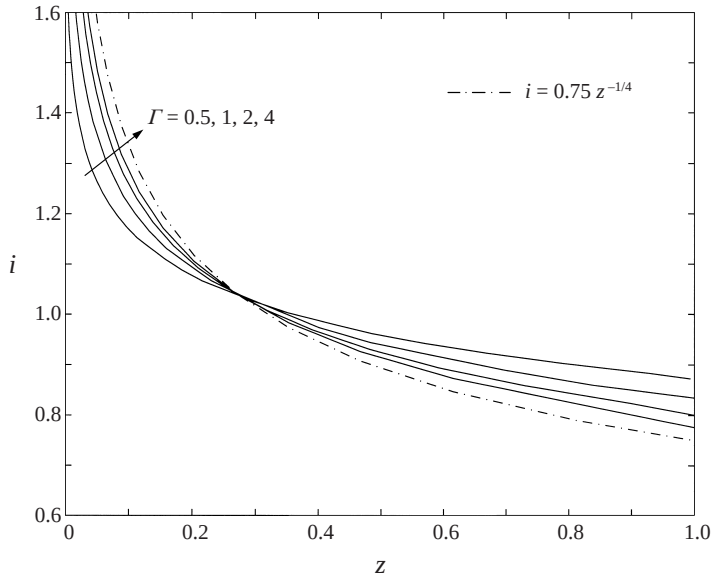

FIGURE 5. Current density distribution, $i(z)$, along the electrode for the same parameters as in figures 2 and 3 and with $\Gamma = 0.5, 1, 2, 4$.

Λ_a	94.9				23.7
Γ	0.5	1	2	4	2
i_o	2.77	4.95	15.9	168	124

TABLE 1. Current density at the lower end of the electrode, i_o, for various values of Λ_a and Γ and with $\Lambda_L = 94.9 \times 10^8$ and $Re_\delta = 0.06$.

distribution. For large Γ a limit current distribution, $i(z) = 0.75z^{-1/4}$, is approached which is also shown in figure 5. (One may see from the formulation in the Appendix that this limit, $\Gamma \to \infty$, corresponds to a similarity solution of the governing equations such that $i_o \to \infty$ which, if (A 3) is disregarded, mathematically is analogous to laminar natural convection along a heated plate.)

Bubble overpotential distributions, $\tilde{\phi}_l(z)$, corresponding to the current distributions presented are shown in figure 6. The negative values represent a loss in catodic polarization as a result of the increased resistivity caused by the bubbles. This must of course be compensated for by the constant part of the total overpotential, Φ_0, defined in (2.21). For the smallest value of Γ shown, i.e. for a comparatively small relative potential drop, the bubble overpotential distribution is continuously changing along the electrode. For the largest value of Γ, $\tilde{\phi}_l$ takes an almost constant negative value along the electrode, except for a small region close to the edge. Apparently, as Γ and thus the potential drop are large, the effective non-dimensional bubble overpotential, $\Gamma\tilde{\phi}_l$, as it appears in the exponent of (3.13), requires only a small relative variation of $\tilde{\phi}_l$ to change the current density at the electrode.

For the case of smaller bubbles, $\Lambda_a = 23.7$, the mechanism of shear-induced diffusion of bubbles is weaker. As can be observed in figure 7, the bubbles do not spread so far from the electrode as in the case of larger bubbles shown in figure 2. The more narrow bubble layer also results in a higher gas volume fraction. (One

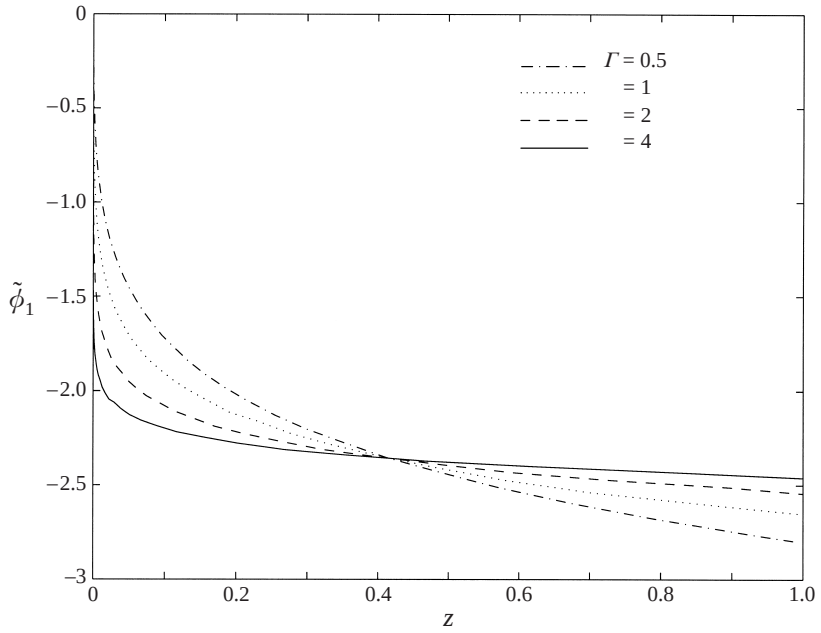

FIGURE 6. Bubble overpotential, $\tilde{\phi}_l$, versus the vertical coordinate for the same parameters as in figures 2 and 3 and with $\Gamma = 0.5, 1, 2, 4$.

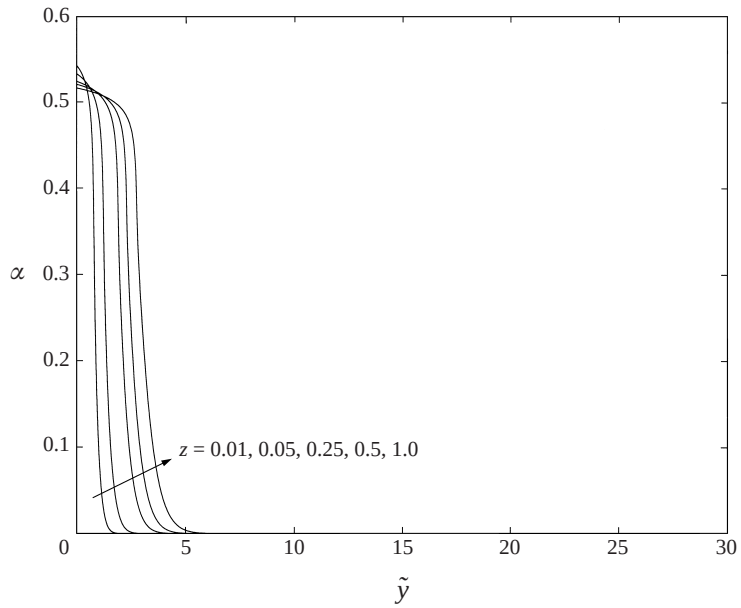

FIGURE 7. Gas volume fraction versus wall-normal coordinate at the vertical positions $z = 0.01, 0.05, 0.25, 0.5, 1.0$ for $Re_\delta = 0.06, \Lambda_a = 23.7, \Lambda_L = 94.9 \times 10^8$ and $\Gamma = 2$.

should bear in mind here the qualitative nature of these results. Incorporation of other dipersion mechanisms in the model may well change the gas volume fraction levels.) The mixture velocity, shown in figure 8, is of the same order of magnitude as for the larger bubbles, but with the maximum of the profile shifted towards the

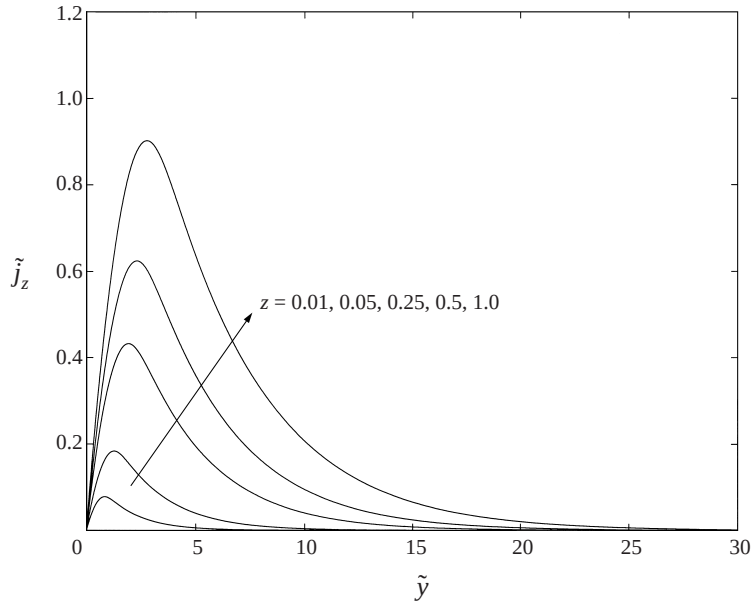

FIGURE 8. Vertical component of mixture velocity versus wall-normal coordinate at the vertical positions $z = 0.01, 0.05, 0.25, 0.5, 1.0$ for $Re_\delta = 0.06, \Lambda_a = 23.7, \Lambda_L = 94.9 \times 10^8$ and $\Gamma = 2$.

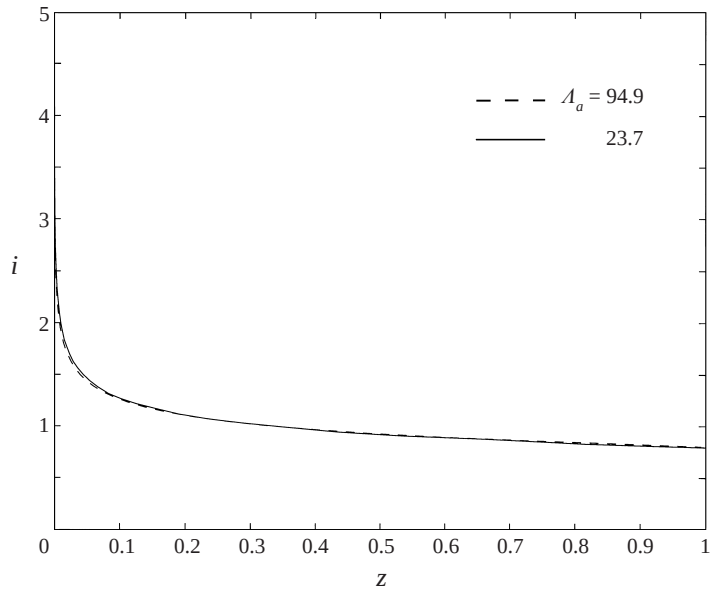

FIGURE 9. Current density distribution, $i(z)$, along the electrode for the cases $\Lambda_a = 23.7$ and $\Lambda_a = 94.9$ with $Re_\delta = 0.06, \Lambda_L = 94.9 \times 10^8$ and $\Gamma = 2$.

electrode. Using the estimates given in § 3.1 for the variables suggest that $\alpha, \tilde{\delta}$ and $\tilde{j}_z$ of the present case for $\Lambda_a = 23.7$ may be obtained by scaling those variables for the previous case, $\Lambda_a = 94.9$, by a factor 1.4, 0.8 and 0.9, respectively. Comparing maximum values of α and $\tilde{j}_z$ and the position of the steepest slope of the volume fraction profiles of the two cases seem to confirm these scaling laws. As the Reynolds

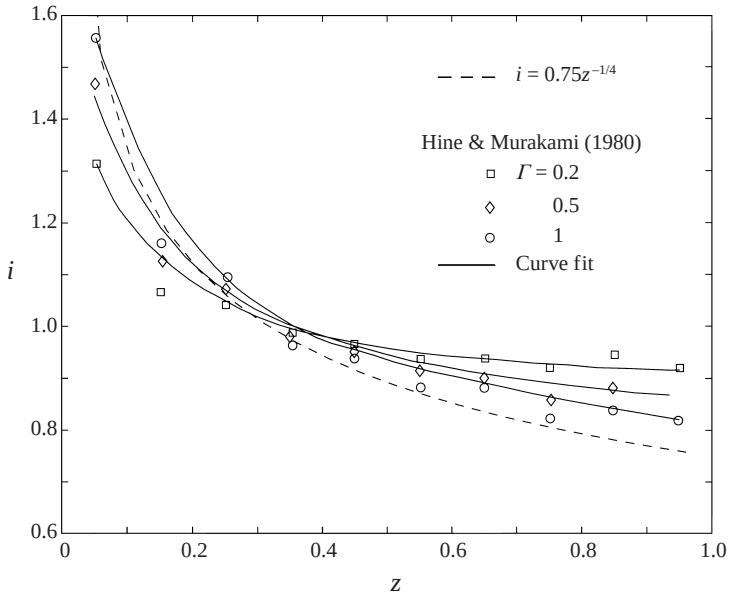

FIGURE 10. Current density distribution, $i(z)$, for the experimental results of Hine & Murakami (1980) in an electrolytic cell with natural circulation; measured and curve fits. $\Gamma = 0.2, 0.5, 1$. (Reproduction by computeraided scanning and copying from printed source.)

number has not changed, $Re_\delta = 0.06$, the thickness of the inertial, bubble-free, outer part of the boundary layer is roughly the same. The development along the electrode of the gas volume fraction at the wall, the maximum of the velocity profile and the distance from the electrode of the maximum are not shown, but are qualitatively similar to the case in figure 4 for $\Lambda_a = 94.9$.

The current density distribution along the electrode for the cases of $\Lambda_a = 23.7$ and $\Lambda_a = 94.9$ are compared in figure 9, which shows that there is hardly any visible difference between them. Table 1 reveals that the former case has an initial value of the current density at the lower end which is about ten times that of the latter. However, this is not apparent from the graph, which essentially demonstrates that the current distribution, at large, is insensitive to the bubble size.

Finally, we make a comparison of our results with the experimental results of Hine & Murakami (1980) for an electrolytic cell with natural circulation. Measured current densities and fitted curves, as reproduced from the printed source, are shown in figure 10. The values of Γ in their experiment, $\Gamma = 0.2, 0.5, 1$, are approximate as calculated from the reported currents used and our estimation of the conductivity of their electrolyte. Values of Λ_a (and Re_δ) are not available but seem less essential for a comparison as is apparent from our results (see figure 9). The qualitative agreement with our computational results in figure 5 is good and a quantitative comparison is surprisingly fair, considering the fact that we model only a single electrode. A direct comparison with the present theory for the case $\Gamma = 1$ is presented in figure 11. In the same figure we also show previous models by Tobias (1959) and Rousar (1969). The model parameter in the former case is that suggested by Hine & Murakami (1980) to fit their data best. In the latter case the model parameter is computed from experimental data as suggested by Vogt (1983), who slightly simplified Rousar's model. The present model definitely seems to agree best with the experimental data.

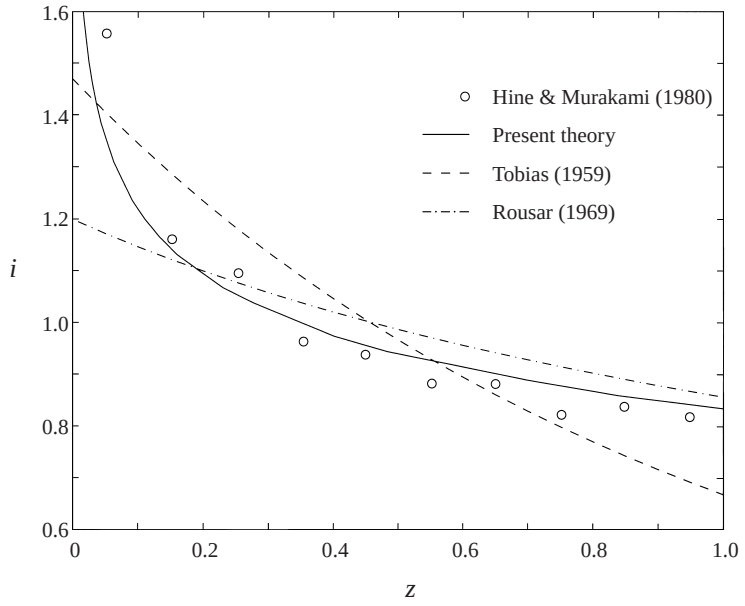

FIGURE 11. Current density distribution, $i(z)$, for $\Gamma = 1$. Circles: experiment of Hine & Murakami (1980); ——: present model; — —: model of Tobias (1959), $i(z) = 8(K+2)^2/(K+4)(2+Kz)^3$, $K = 0.6$; — · —· : model of Rousar (1969), $i(z) = (1+C)/(4z(1+C)+C^2)^{1/2}$, $C = 5$.

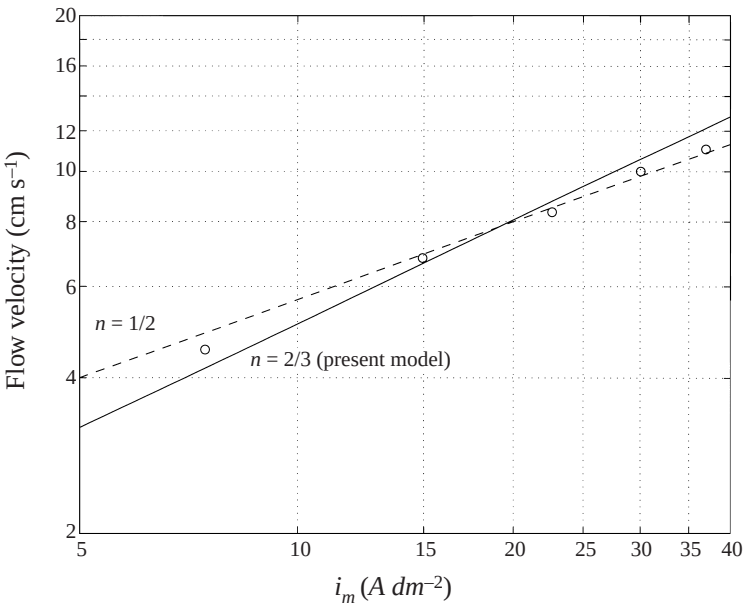

FIGURE 12. Average flow velocity (cm s^{-1}) versus average current density (A dm^{-2}). Circles: experiment of Hine & Murakami (1980); ——: present scaling law, $j_z \sim i_m^{2/3}$; - - -: scaling law of Hine & Murakami (1980), $j_z \sim i_m^{1/2}$.

A comparison of the estimated thickness of their velocity boundary layer from our analysis, $\delta \sim 7$ mm (at the end of the 890 mm long channel), with the channel width, 19 mm, indicates that the channel flow might partly be that of two non-merged boundary layers. One should bear in mind though, that our computational results

lack not only the more restricted flow domain of the experiment, but also the bubbles and corresponding boundary layer at the counter-electrode. Still, our model seems to capture the essentials of a description of the current distribution. Figure 12 shows the measured average flow velocity at the bottom of the cell versus the average current density at the electrodes and, for comparison, two different scaling laws of the velocity. Hine & Murakami (1980) proposed that the dimensional velocity $j_z \sim i_m^{1/2}$ whereas our model, for a single electrode, suggests $j_z \sim i_m^{2/3}$. The agreement of the present scaling with the experimental results is fair, but not better than that suggested by Hine & Murakami (1980).

5. Conclusions

We considered the modelling of two-phase flow adjacent to a single, vertical, gas-evolving electrode at large catodic polarization in a binary electrolyte. The rate of gas evolution was coupled to the electrochemistry through Faraday's law and through the charge transfer rate at the electrode surface, which is a strong nonlinear function of the overpotential at the liquid–electrode interface. A buoyant boundary layer of thickness $\delta \sim L(\nu_C j_{H_2 m}/gL^2)^{1/3}$ was predicted by the model, which treated the bubble–liquid mixture as a monodisperse suspension of light particles. Existing empirical models for shear-induced diffusion and hydrodynamic self-diffusion of particles were employed to describe the dispersal of bubbles through the liquid. The presence of a shear-induced hydrodynamic gradient diffusion of the ionic species indicated a drastically enhanced mass transport in comparison to molecular diffusion. This gives rise to the proposal that only small relative variations in the species concentration,

$$\frac{\Delta c}{c_0} \sim \left(\frac{\nu_C j_{H_2 m}}{g a^2}\right)^{1/4} \frac{p_{H_2}}{c_0 \mathscr{R} T},$$

occur.

The predicted current density was shown to be approximately constant throughout the boundary layer but strongly non-uniform along the electrode. The decreased conductivity of the electrolyte in the thickening bubble layer concentrated the current density, and thereby the generation of gas, at the lower end of the electrode. The ratio $ga^2/\nu_C j_{H_2 m}$ estimates the ratio of the shear-induced flux of bubbles to that which results from advection by the gas injection velocity. The current density distribution was essentially insensitive to this parameter although the thickness of the bubble plume decreased for smaller values of it. This suggests that more elaborate models for the bubble transport mechanisms may not be critical for the description of current density distribution. On the other hand, larger values of $(i_m \delta/\sigma_C^0)/(\mathscr{R}T/F)$, which measures the relative potential drop in the boundary layer, tended to increase the non-uniformity of the current density.

Although the model presented lacks completeness in the detailed physical description of the bubble and ionic species transport mechanisms, it does account for some of the fundamental physical phenomena of a gas-evolving electrode in laminar flow conditions. The predicted current density distributions along the electrode indeed show good agreement with experimental results from the literature. The results also serve to demonstrate a good ability of our method to numerically handle the somewhat unusual and strongly nonlinear boundary condition that appears from the electrode kinetics. The results give encouragement for any future studies of a complete narrow

electrolytic cell, and possibly including a more complete set of bubble dispersion mechanisms in the model and accounting for the ionic species variations.

Appendix. Iteration procedure

To formulate the iteration procedure for the numerical solution of the boundary layer equations we first introduce streched coordinates:

$$\eta = \tilde{y}/z^{1/4}, \quad \zeta = z i_o^4. \tag{A 1a,b}$$

The wall-normal coordinate is introduced in analogy with the case of natural laminar convection along a heated plate. Secondly, by defining the normalized current density distribution,

$$I(z) = \frac{i(z)}{i_o}, \tag{A 2}$$

elimination of $\tilde{\phi}_l$ between (3.19) and (3.13) and using the new variables yields

$$I(\zeta) = (1 - \alpha_l(\zeta)) \exp\left(-\frac{\Gamma}{2} I(\zeta)\zeta^{1/4} k(\zeta)\right), \tag{A 3}$$

where

$$k(\zeta) = \int_0^\infty \frac{1 - g(\alpha(\zeta,\eta))}{g(\alpha(\zeta,\eta))}\,\mathrm{d}\eta, \tag{A 4}$$

and where i_o, by (3.21), satisfies

$$i_o = i_o^4 \Big/ \int_0^{i_o^4} I(\zeta)\,\mathrm{d}\zeta. \tag{A 5}$$

The non-dimensional electric potential in these variables is $\tilde{\phi}_l = -I(\zeta)\zeta^{1/4}k(\zeta)$. A stream function,

$$\Psi = z^{3/4} F(\zeta,\eta), \tag{A 6}$$

is introduced, where $F(\zeta,\eta)$ is the scaled boundary layer stream function. The velocity components are

$$\tilde{j}_z = \frac{\partial \Psi}{\partial \tilde{y}} = \frac{\zeta^{1/2}}{i_o^2}\frac{\partial F(\zeta,\eta)}{\partial \eta}, \tag{A 7}$$

$$\tilde{j}_y = -\frac{\partial \Psi}{\partial z} = i_o\left[-\frac{\partial}{\partial \zeta}(\zeta^{3/4}F(\zeta,\eta)) + \frac{\zeta^{-1/4}}{4}\eta\frac{\partial F(\zeta,\eta)}{\partial \eta}\right]. \tag{A 8}$$

The boundary layer equations, (3.4), (3.5), formulated with the new variables and with partial derivatives denoted by subscripts ζ and η respectively, are then

$$\zeta\alpha_\zeta F_\eta - \zeta F_\zeta \alpha_\eta - \tfrac{3}{4}\alpha_\eta F = \Lambda_a\left(\frac{\zeta^{1/4}}{i_o}\beta(\alpha)|F_{\eta\eta}|\alpha_\eta + \frac{1}{3}\frac{\Lambda_a^{1/2}}{\Lambda_L^{1/6}}D_\perp\alpha_\eta\right)_\eta, \tag{A 9}$$

$$\begin{aligned} &Re_\delta(1-\alpha)\left(\zeta F_{\eta\zeta}F_\eta - \zeta F_\zeta F_{\eta\eta} + \tfrac{1}{2}F_\eta^2 - \tfrac{3}{4}F_{\eta\eta}F\right) \\ &\quad + Re_\delta F_{\eta\eta}\Lambda_a\left(\frac{\zeta^{1/4}}{i_o}\beta(\alpha)|F_{\eta\eta}|\alpha_\eta + \frac{1}{3}\frac{\Lambda_a^{1/2}}{\Lambda_L^{1/6}}D_\perp\alpha_\eta\right) = \alpha + (\mu(\alpha)F_{\eta\eta})_\eta. \end{aligned} \tag{A 10}$$

The boundary conditions at the electrode, (3.10), are

$$F_\eta(\eta=0)=0, \quad F(\eta=0)=-\zeta^{-3/4}\int_0^\zeta I(\zeta')\,\mathrm{d}\zeta', \tag{A 11}$$

$$-\Lambda_a\left(\frac{\zeta^{1/4}}{i_o}\beta(\alpha)\,|F_{\eta\eta}|\,\alpha_\eta+\frac{1}{3}\frac{\Lambda_a^{1/2}}{\Lambda_L^{1/6}}D_\perp\alpha_\eta\right)_{\eta=0}=\zeta^{1/4}I(\zeta)(1-\alpha_l), \tag{A 12}$$

where the second expression in (A 11) is obtained from (3.10) and (A 8) by formal integration, and $I(\zeta)$ is given implicitly by (A 3). Far away from the electrode

$$F_\eta(\eta\to\infty)\to 0, \quad \alpha(\eta\to\infty)\to 0. \tag{A 13}$$

Now, with an initial guess, i_o^{old} say, and since $I(0)=1$, (A 9), (A 10), (A 11), (A 12) and (A 3) can be integrated numerically from the lower end of the plate. The marching is continued until the end of the plate at $z=1$, which corresponds to $\zeta=i_o^4$. The latter relation will be used to define a new guess $i_o^{new}=\zeta_{max}^{1/4}$, where ζ_{max} is obtained from

$$\int_0^{\zeta_{max}} I(\zeta)\,\mathrm{d}\zeta=\zeta_{max}^{3/4}, \tag{A 14}$$

which follows directly from (A 5) and the definition of ζ_{max}. Thus, the integration along the plate is continued for each iteration sweep until (A 14) is satisfied for some value of $\zeta>0$. The procedure is then repeated until convergence is achieved.

The numerical integration of the boundary layer equations, with specified i_o^{old} in (A 9), (A 10) and (A 12), is based on a finite difference scheme proposed by Harris & Blanchard (1982). The discretization is progressively made in the direction along the electrode so that $\zeta_{n+1}/\zeta_n=constant$, where n is a mesh index starting at the lower end. Finite difference discretizations of the various terms of the equations follow closely those given by Harris & Blanchard (1982) and are not given here. A non-standard feature, though, is the implicit algebraic relation (A 3) which determines $I(\zeta_{n+1})$ in each integration step. For this, a nested Newton–Raphson iteration procedure was implemented in each step. Let $\mathscr{I}$, as proposed by (A 3), be the solution to

$$\mathscr{I}=(1-\tilde{\alpha}_l(\zeta_{n+1}))\,\exp\left(-\frac{\Gamma}{2}\mathscr{I}\zeta_{n+1}^{1/4}\tilde{k}_{n+1}\right), \tag{A 15}$$

where

$$\tilde{k}_{n+1}=\int_0^\infty\frac{1-g(\tilde{\alpha}(\zeta_{n+1}))}{g(\tilde{\alpha}(\zeta_{n+1}))}\,\mathrm{d}\eta, \tag{A 16}$$

and, disregarding (A 3), $\tilde{\alpha}(\zeta_{n+1})$ is obtained from the solution of integration step $n+1$ with any specified value of the normalized current density, $\tilde{I}(\zeta_{n+1})$ say, in the boundary conditions (A 11) and (A 12). The Newton–Raphson method is then formulated to find the zero of $\mathscr{F}=\tilde{I}(\zeta_{n+1})-\mathscr{I}[\tilde{I}(\zeta_{n+1})]$, whereby each integration step is repeated iteratively until $\mathscr{F}=0$. In turn, each Newton–Raphson iteration requires the solution of (A 15) for $\mathscr{I}$, which is conveniently obtained by an additional, inner Newton–Raphson loop.

An approximate similarity solution is available for small values of ζ, which is used to start the numerical integration of the full solution. This is presented elsewhere, Dahlkild (2000), together with a physical description and mathematical formulation for the very early stages of the developing boundary layer.

REFERENCES

Achard, J. L. & Cartellier, A. 1985 Local characteristics of upward bubbly flows. *Physico Chem. Hydrodyn.* **6**, 841–852.

Acrivos, A. & Herbolzheimer, E. 1979 Enhanced sedimentation in settling tanks with inclined walls. *J. Fluid Mech.* **92**, 435–457.

Antal, S. P., Lahey, R. T. & Flaherty, J. E. 1991 Analysis of phase distribution in fully developed laminar bubbly two-phase flow. *Intl J. Multiphase Flow* **17**, 635–652.

Atkinson, G. 1972 Electrochemical information. In *American Institute of Physics Handbook*, 3rd edn (ed. D. E. Gray), pp. 5-249–5-263. McGraw-Hill.

Bockris, J. O'M. & Reddy, A. K. N. 1977 In *Modern Electrochemistry*, Vol. 2, Plenum.

Boissonneau, P. & Byrne, P. 2000 An experimental investigation of hydrogen gas bubbles-induced free convection in a small electrochemical cell. *J. Appl. Electrochem.* **30**, 767–775.

Bruggeman, D. A. G. 1935 Berechnung verschiedener physikalisher Konstanten von hetrogenen Substanzen. I. *Ann. Phys.* **24**, 659.

Byrne, P., Simonsson, D., Lucor, D. & Fontes, E. 1999 A model of the anode from the clorate cell. In *Fluid Mechanics and its Applications. Transfer phenomena in Magnetohydrodynamic and Electroconducting Flows*, Vol. 51 (ed. A. Alemany, P. Marty & J. P. Thibault). Kluwer.

Chapman, B. K. & Leighton, D. T. 1991 Dynamic viscous resuspension. *Intl J. Multiphase Flow* **17**, 469–483.

Dahlkild, A. A. 2000 Modelling the current distribution and two-phase flow along a vertical, gas-evolving hydrogen electrode. *TRITA-MEK Tech. Rep.* 2000:12. ISSN 0348-467X, ISRN KTH/MEK/TR–00/12–SE.

Davis, R. H. & Hassen, M. A. 1988 Spreading of the interface at the top of a slightly polydisperse sedimenting suspension. *J. Fluid Mech.* **196**, 107–134, and Corrigendum **202** (1989) 598–599.

Drew, D. A. 1990 The plane Poiseuille flow of a particle-fluid mixture. *Trans. ASME: J. Fluids Engng* **112**, 362–366.

Drew, D. A. & Lahey, R. T. 1987 The virtual mass and lift force on a sphere in rotating and straining inviscid flow. *Intl J. Multiphase Flow* **14**, 113–121.

Funk, J. E. & Thorpe, J. F. 1969 Void fraction and current density distributions in a water electrolysis cell. *J. Electrochem. Soc.* **116**, 48–54.

Ham, J. M. & Homsy, G. M. 1988 Hindered settling and hydrodynamic dispersion in quiscent sedimenting suspensions. *Intl J. Multiphase Flow* **14**, 533–546.

Harris, J. E. & Blanchard, D. K. 1982 Computer program for solving laminar, transitional, or turbulent compressible boundary-layer equations for two-dimensional and axisymmetric flow. *NASA Tech. Mem.* 83207.

Hine, F. & Murakami, K. 1980 Bubble effects on the solution IR drop in a vertical electrolyser under free and forced convection. *J. Electrochem. Soc.* **127**, 292–297.

Ho, B. P. & Leal, L. G. 1974 Inertial migration of rigid spheres in two-dimensional unidirectional flows. *J. Fluid Mech.* **65**, 365–400.

Ishii, M. 1975 *Thermo Fluid Dynamic Theory of Two-Phase Flow*. Eyrolles.

Ishii, M. & Zuber, N. 1979 Drag coefficient and relative velocity in bubbly, droplet or particulate flows. *AIChE J.* **25**, 834–855.

Janssen, L. J. J. 1978 Mass transfer at gas evolving electrodes. *Electrochimica Acta* **23**, 81–86.

Janssen, L. J. J. 1989 Behaviour of and mass transfer at gas-evolving electrodes. *Electrochimica Acta* **34**, 161–169.

Kashinsky, O. N., Timkin, L. S. & Cartellier, A. 1993 Experimental study of laminar bubbly flows in a vertical pipe. *Expts. Fluids* **15**, 308–314.

Koch, D. L. 1996 Hydrodynamic diffusion near solid boundaries with applications to heat and mass transport into sheared suspensions and fixed fibre beds. *J. Fluid Mech.* **318**, 31–47.

Leighton, D. & Acrivos, A. 1987*a* Measurements of shear-induced self-diffusion in concentrated suspensions of spheres. *J. Fluid Mech.* **177**, 843–855.

Leighton, D. & Acrivos, A. 1987*b* The shear-induced migration of particles in concentrated suspensions. *J. Fluid Mech.* **181**, 415–439.

Lukowzew, P., Lewina, S. & Frumkin, A. 1939 Hydrogen overvoltage on nickel. *ACTA Physic-ochimica URSS* **XI**, No. 1, 21–44.

Marrucci, G. & Nicodemo, L. 1967 Coalescence of gas bubbles in aqueous solutions of inorganic electrolytes. *Chem. Engng Sci.* **22**, 1257–1265.

Nakoryakov, V. E., Kashinsky, O. N., Randin, V. V. & Timkin, L. S. 1996 Gas-liquid bubbly flow in vertical pipes (Data bank contribution). *Trans. ASME: J. Fluids Engng* **118**(2), 377–382.

Nicolai, H., Herzhaft, B., Hinch, E. J., Oger, L. & Guazzelli, E. 1995 Particle velocity fluctuations and hydrodynamic self-diffusion of sedimenting non-Brownian spheres. *Phys. Fluids* **7**, 12–23.

Nir, A. & Acrivos, A. 1990 Sedimentation and sediment flow on inclined surfaces. *J. Fluid Mech.* **212**, 139–153.

Rousar, I. 1969 Calculation of current density distributions and terminal voltage for bipolar electrolyzers; application to chlorate cells. *J. Electrochem. Soc.* **116**, 676–683.

Rousar, I., Cezner, V., Nejepsova, J., Jacksic, M. M., Spasojevic, B. Z. & Nikolic, B. Z. 1977 Calculation of local current densities and terminal voltage for a monopolar sandwich electrolyzer: application to chlorate cells. *J. Appl. Electrochem.* **7**, 427–435.

Saffman, P. G. 1965 The lift on a sphere in a slow shear flow. *J. Fluid Mech.* **22**, 285–400.

Schaflinger, U. 1996 Laminar transport of solid particles suspended in liquids. In *The Flow of Particles in Suspensions* (ed. U. Schaflinger). Springer.

Tobias, C. W. 1959 Effect of gas evolution on current distribution and ohmic resistance in electrolyzers. *J. Electrochem. Soc.* **106**, 833–838.

Wang, Y., Mauri, R. & Acrivos, A. 1996 The transverse shear-induced liquid and particle tracer diffusivities of a dilute suspension of spheres undergoing a simple shear flow. *J. Fluid Mech.* **327**, 255–272.

Wedin, R. 1999 Numerical studies of two-phase flows in gas-evolving electrochemical applications. *TRITA-MEK Tech. Rep.* 1999:03. Licentiate thesis, KTH. ISRN KTH/MEK/TR-99/03-SE.

Vetter, K. J. 1967 *Electrochemical Kinetics.* Academic.

Vogt, H. 1981 A hydrodynamic model for the ohmic interelectrode resistance of cells with vertical gas evolving electrodes. *Electrochimica Acta* **26**, No. 9, 1311–1317.

Vogt, H. 1983 Gas evolving electrodes In *Comprehensive Treaties of Electrochemistry*. (ed. E. Yeager, B. E. Bockris, B. E. Conway & S. Sarangapani), pp. 445–489. Plenum.